

## **Influence of Inherent Anisotropic Stiffness Induced Degradation on Articular Surface**

**Boonyong Punantapong<sup>1\*,2</sup>, Somchai Thongtem<sup>1</sup>, Michael J. Fagan<sup>3</sup>  
and Chairroj Soorapanth<sup>4</sup>**

<sup>1</sup> Faculty of Science, Chiang Mai University, Chiang Mai 50200, Thailand

<sup>2</sup> Faculty of Applied Science, King Mongkut's Institute of Technology North Bangkok, Bangkok 10800, Thailand

<sup>3</sup> Centre for Medical Engineering and Technology, University of Hull, Hull, UK

<sup>4</sup> Department of Orthopedic Surgical, Bangkok Metropolitan Administration Medical College and Vajira Hospital, Bangkok 10300, Thailand

\*Corresponding author. E-mail: [bpp@kmitnb.ac.th](mailto:bpp@kmitnb.ac.th)

### **ABSTRACT**

*The role of viscoelasticity of collagen fibers in articular cartilage was examined in compression and tension, using stress relaxation measurements in axial direction (normal to the articular surface). In this study, the degree of inherent stiffness anisotropy of completely-decomposed element was evaluated using finite element method. The model accounted for elastic deformations of the nanostructure in contact and assumed laminar flow in the created voids. The stiffness parameters from the laboratory tests were utilized in analysis which the elasticity of the solid phase was investigated in the present study. The results were suggested that the dominant mechanism for stress relaxation arose from fluid pressurization, while the associated relaxation in collagen fibers mainly was resulted in an increase in radial strain. Furthermore, Young's modulus normal to the contact surface was increased from the superficial to the deep zone in articular cartilage.*

**Key words:** Stiffness, Degradation, Articular surface

### **INTRODUCTION**

Articular cartilage consists of three major structural constituents: collagen fibers, proteoglycan matrix and interstitial water. The function of articular cartilage serves mainly as a load-bearing medium in joints, thus the structure of cartilage is customarily designed to carry high stresses. Articular cartilage is a poroelastic material consisting of a fluid component (75% wet weight) and a solid matrix (20–25% wet weight), which the solid phase of articular cartilage is mainly composed of collagen (65%), proteoglycan (25%), glycoprotein and chondrocytes (<10%), and lipid (<10%) (Minns and Steven, 1977; Stockwell, 1979; Jones et al., 1997).

Recent developments in mathematical modeling have improved the understanding of cartilage mechanics, such as Mow et al.,(1980), Holmes and Mow (1990), Guilak et al.,(1995), Garcia et al.,(1998), and Donzelli et al.,(1999). They have suggested that the proteoglycans are negatively-charged and produce a swelling pressure that depends on the saline concentration of the fluid. At equilibrium and physiological conditions, the swelling pressure is counteracted by the external load and the structural elements in the solid matrix, mainly the collagen fibers. Since collagen fibers, chondrocytes and the other components in the solid

phase have different and distinctly-directional material properties, then articular cartilage is a composite with anisotropic material properties.

However, the importance of collagen fibers for the mechanical function and integrity of cartilage has been demonstrated experimentally by Kwan et al., (1990), Sasaki and Odajima (1996), Khalsa and Eisenberg (1997), and Li and Herzog (2004). At the same time, the stress relaxation and responses of articular cartilage have been observed in many testings where the viscoelasticity is attributed primarily to the collagen fibers, as have been found for other soft tissues in tension and compression (Lee and Rowe, 1989; Pin et al., 1997; Huang et al., 2001; Missirilis and Spiliotis, 2002). So it is well accepted that chondrocytes play an important role in cartilage adaptation and degeneration. The mechanical environment of chondrocytes can stimulate and regulate the biosynthetic activities in the cell.

Furthermore, Minns and Steven (1977) were found that the articular cartilage can be divided into three distinct morphological zones as superficial zone, middle zone and deep zone. In the superficial zone (10–20% of the total thickness), collagen fibers are oriented parallel to the articular surface. While in the middle zone (40–60% of the total thickness), there is no preferred orientation for the collagen fibers, and in the deep zone (30% of the total thickness), the collagen fibers are approximately perpendicular to the articular surface. In normal cartilage, chondrocytes change shape across the thickness (Guilak et al., 1995): chondrocytes are typically flattened in the surface zone, spherical in the middle zone and arranged in columns in the deep zone. The distribution of chondrocytes in cartilage is not uniform: the average cell volumetric concentration increases from the deep zone to the surface zone by a factor of about three (Jones et al., 1997).

The purpose of this study was to investigate the effects of the structural arrangement of the collagen fiber network and distribution of stress-strain on the global material behavior of articular cartilage by using finite element method. So, the effective material properties of articular cartilage was assumed to be a four-phasic composite of a proteoglycan matrix, vertically-and horizontally-distributed collagen fiber, and spheroidal inclusions representing chondrocytes (Qiu and Weng, 1990).

## MATERIALS AND METHODS

Because of the great difference in material properties between proteoglycan matrix, cells and collagen fibers, cartilage is not a uniform material. In order to include these structural, non-uniform effects, cartilage has been represented using a transversely-isotropic material (e.g., Garcia et al., 1998; Donzelli et al., 1999). So, the global material properties have not been related to the microstructure of the tissue. Li and Herzog (2004) investigated theoretically the effects of the collagen fiber network on anisotropy of cartilage properties. In their models, the effect of volumetric concentration of collagen fibers, the structure of the fiber network, and the distributed chondrocytes were not included. Since the material anisotropy of cartilage is likely caused by microstructural variations in the tissue, i.e., the distribution of cartilage fibers and chondrocytes, the description of cartilage using a uniform, transversely isotropic model is not appropriate.

However, in this study, we used axisymmetrical model to simulate the behavior of the cross-anisotropic elastic material in which the horizontal plane is isotropic, and denoting axes  $x$  and  $y$  as the horizontal directions, and axis  $z$  as the vertical directions, as shown in Figure 1 and Figure 2. Then the effective stress-strain relationship of the element can be described. If the stress-strain behavior is governed by five independent elastic parameters:  $E_v$ ,  $E_h$ ,  $G_{vh}$  ( $=G_{hv}$ ),  $\nu_{vh}$ , and  $\nu_{hh}$ , where  $E_v$  and  $E_h$  are the Young's moduli in the vertical and horizontal directions, respectively;  $G_{vh}$  ( $=G_{hv}$ ) is the elastic shear modulus in any vertical

plane;  $\nu_{vh}$  is the Poisson's ratio for the effect of vertical strain on horizontal strain; and  $\nu_{hh}$  is the Poisson's ratio for the effect of horizontal strain on the complementary horizontal strain. Then the relationship of stress-strain can be written by the following (Lee and Rowe, 1989).

$$\begin{pmatrix} \delta\varepsilon_{h1} \\ \delta\varepsilon_{h2} \\ \delta\varepsilon_v \\ \delta\gamma_{hv} \\ \delta\gamma_{vh} \\ \delta\gamma_{hh} \end{pmatrix} = \begin{pmatrix} \frac{1}{E_h} & \frac{-\nu_{hh}}{E_h} & \frac{-\nu_{vh}}{E_v} & 0 & 0 & 0 \\ \frac{-\nu_{hh}}{E_h} & \frac{1}{E_h} & \frac{-\nu_{vh}}{E_v} & 0 & 0 & 0 \\ \frac{-\nu_{vh}}{E_v} & \frac{-\nu_{vh}}{E_v} & \frac{1}{E_v} & 0 & 0 & 0 \\ 0 & 0 & 0 & \frac{1}{G_{hv}} & 0 & 0 \\ 0 & 0 & 0 & 0 & \frac{1}{G_{hv}} & 0 \\ 0 & 0 & 0 & 0 & 0 & \frac{2(1+\nu_{hh})}{E_h} \end{pmatrix} \begin{pmatrix} \delta\sigma_{h1} \\ \delta\sigma_{h2} \\ \delta\sigma_v \\ \delta\tau_{hv} \\ \delta\tau_{vh} \\ \delta\tau_{hh} \end{pmatrix} \quad (1)$$

where  $G_r(t)$   $\delta\varepsilon_{h1}$  and  $\delta\varepsilon_{h2}$  are the incremental horizontal strains in the  $h_1$  and  $h_2$  directions, respectively;  $\delta\varepsilon_v$  is the incremental vertical strain;  $\delta\sigma_{h1}$  and  $\delta\sigma_{h2}$  are the incremental effective horizontal stresses in the  $h_1$  and  $h_2$  directions ( $x$  and  $y$  directions), respectively;  $\delta\sigma_v$  is the incremental effective vertical stress;  $\delta\gamma_{hv}$  is the incremental shear strain in the  $h-v$  plane;  $\delta\gamma_{vh}$  is the incremental shear strain in the  $v-h$  plane;  $\delta\gamma_{hh}$  is the incremental shear strain in the  $h-h$  plane;  $\delta\tau_{hv}$  is the incremental shear stress in the  $h-v$  plane;  $\delta\tau_{vh}$  is the incremental shear stress in the  $v-h$  plane; and  $\delta\tau_{hh}$  is the incremental shear stress in the  $h-h$  plane.

For the model simulation, we used ANSYS finite element code for analysis under the conditions of finite deformation kinematics. The material was considered to be elastic-plastic. Isotropic linear elasticity was assumed, combined with isotropic hardening. An axisymmetric model with 9,800 eight-node elements with reduced integration was used to model a quadrant of the 3D indentation process (based on symmetry). The indenter itself is modeled using two four-node tetrahedral elements which are purely elastic with the stiffness much greater than that of the indented material. In Figure 2, several levels of mesh refinement are used in the model to give a very fine mesh near the contact zone. In this region, the stress field can be accurately determined. The conical indenter is modeled as a rigid surface which rotated about the axis of symmetry. A convergence study was performed to ensure that the final result was not mesh-dependent.

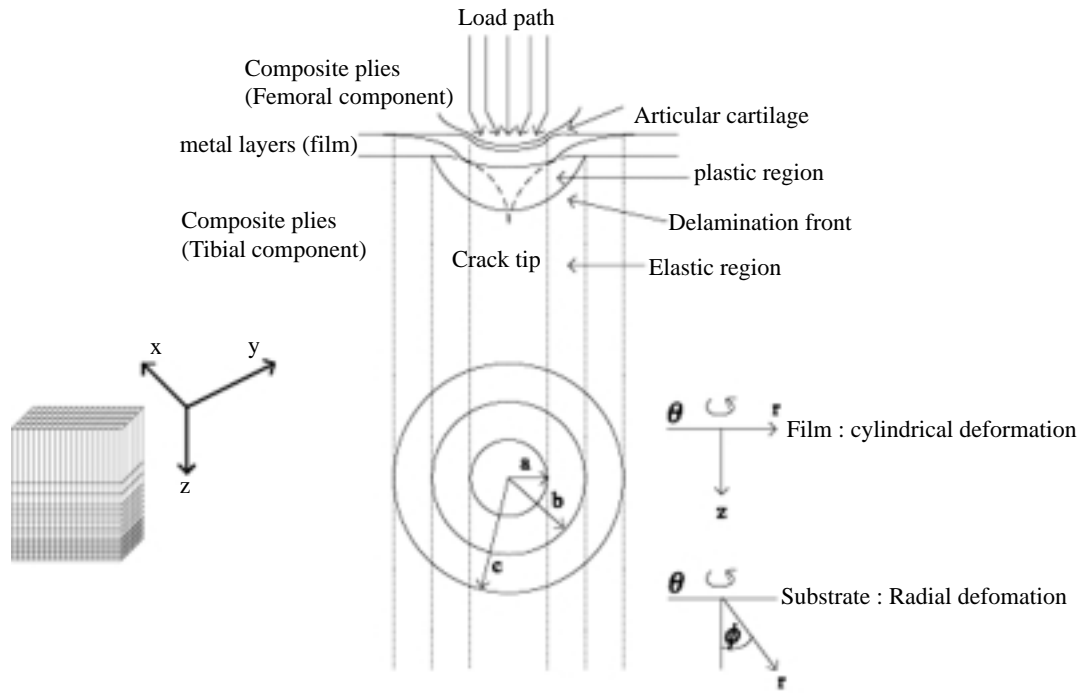


**Figure 1.** Diagram of indentation model on articular cartilage.

At the same time, a fibril-reinforced model (Huang et al., 2001; Li and Herzog, 2004) was used, which consisted of a fluid-saturated elastic matrix and a collagen viscoelastic matrix. Next, the properties of cartilage (Mow et al., 1980; Guilak et al., 1995; Missirilis and Spiliotis, 2002) were defined by three strain-dependent tensile moduli of the fibrillar matrix for the coordinate directions,  $E_r^f(\epsilon_r)$ ,  $E_\theta^f(\epsilon_\theta)$ ,  $E_z^f(\epsilon_z)$  as the model tested. Thus the fibers are in tension, the fibrillar stresses are determined by the hereditary integrals. For the radial ( $r$ ) direction, we obtained

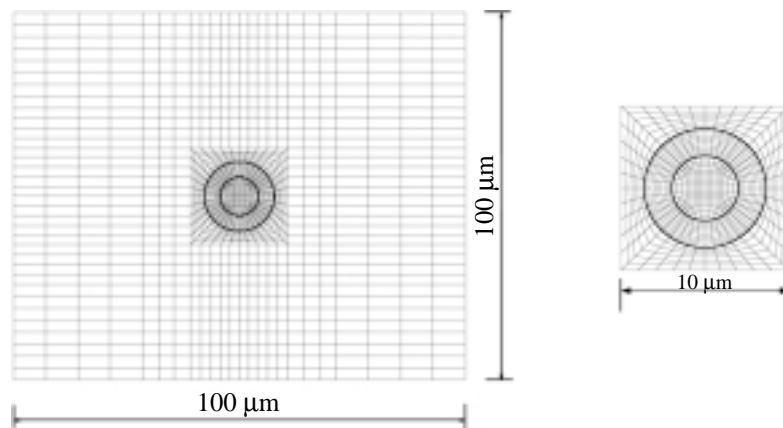


**Figure 2.** The model of axisymmetric model of single cell within the articular surface.

$$\sigma_r^f(t) = \sigma_r^f(0) + \int_0^t G_r(t-\tau) E_r^f(\epsilon_r) \epsilon_r d\tau \tag{2}$$

where  $\epsilon_r$  is the radial strain,  $\epsilon_z$  is the axial strain,  $\sigma_r$  is the radial stress,  $\sigma_z$  is the axial

stress,  $E_r^f$  is the fibrillar modulus

Furthermore, Li and Herzog (2004) were found that the viscoelastic dissipation of the radial fibers had relatively more influence on the compressive load response in early relaxation. In late relaxation, the actual fibrillar modulus ( $G_r(t)E_r^f$ ) was reduced considerably, resulting in an increase in the radius strain. So, the axial and radial stresses of the proteoglycan matrix at equilibrium are

$$\sigma_z = E_m \varepsilon_z + 2\nu_m \sigma_r^m \tag{3}$$

and 
$$\sigma_r^m = -\frac{1}{2} \left[ E_r^f(0) + E_r^f(\varepsilon_r) \right] \varepsilon_r \tag{4}$$

This formulation, to some extent, accounts for nonlinear viscoelasticity, because of the strain-dependence of the modulus (while  $G_r$  is independent on the strain and strain rate). The relaxation function is represented by a discrete spectrum approximation.

$$G_r(t) = 1 + \sum_m g_m \exp\left(\frac{-t}{\lambda_m}\right) \tag{5}$$

Here,  $\lambda_m$  is characteristic times for the viscoelastic dissipation and  $g_m$  is dimensionless constants.

### RESULTS AND DISCUSSION

For the computation, we were used axisymmetric FEA models of knee joint which the articular cartilage layers of the tibial and femoral condyles, and the bone underlying the articular cartilage of the tibia plateau were included. As in the study, we assumed that the permeability of the articular cartilage was strain-dependent. So, the model was implemented in ANSYS code, it consisted of 9,800 elements. The elements in the area under the contact surface had a characteristic length 1–15 nm. This can lead to initial mismatch between the FE model and test results at indentation depths closed to the radius magnitude.

In the test of the contact of a cartilage surface, the reaction forces predicted for the stress-relaxation tests were based on infinitesimal strain theory (Khalsa and Eisenberg, 1997; Donzelli et al., 1999). When a step load was applied to the articular cartilage and this load was increasingly different with increasing time, then the solutions approached the elastic solution and the interstitial fluid was pushed out of the cartilage tissue. Figure 3 illustrates the reaction force predicted using ANSYS for a test with an axisymmetrical joint model, which the material properties and geometry used in the simulations were Young’s modulus,  $E_s = 0.55$  MPa, the cartilage layer thickness,  $b = 0.5$  mm, the radius of curvature of the contacting surface,  $r = 25$  mm, and the compression ratio,  $e = 3$ –10%. The results showed that the reaction force was varied by the compression ratio and the permeability of the cartilage which depends on the deformation state of the cartilage. Thus, this analytical solutions are in good agreement for small trains (compression ratio,  $e$  is smaller than 10%) and for limited time periods.

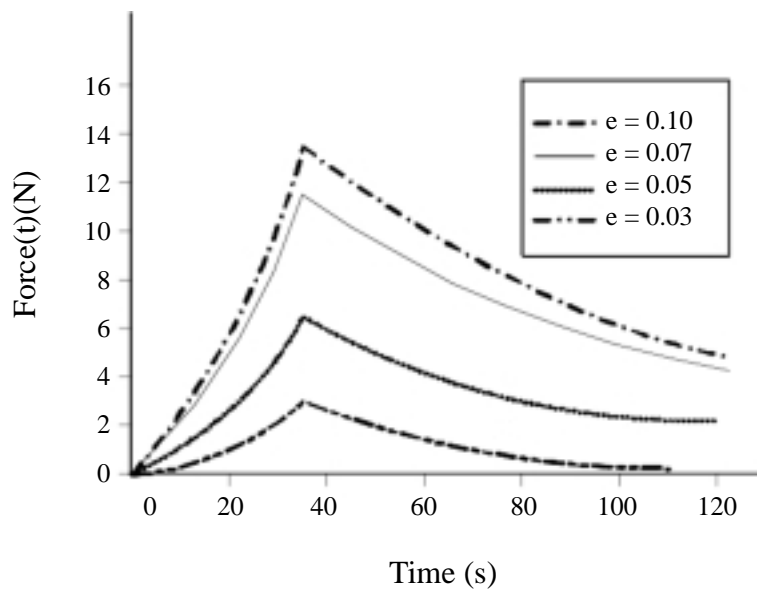


**Figure 3.** The reaction force predicted using ANSYS for a test with an axisymmetrical joint model.

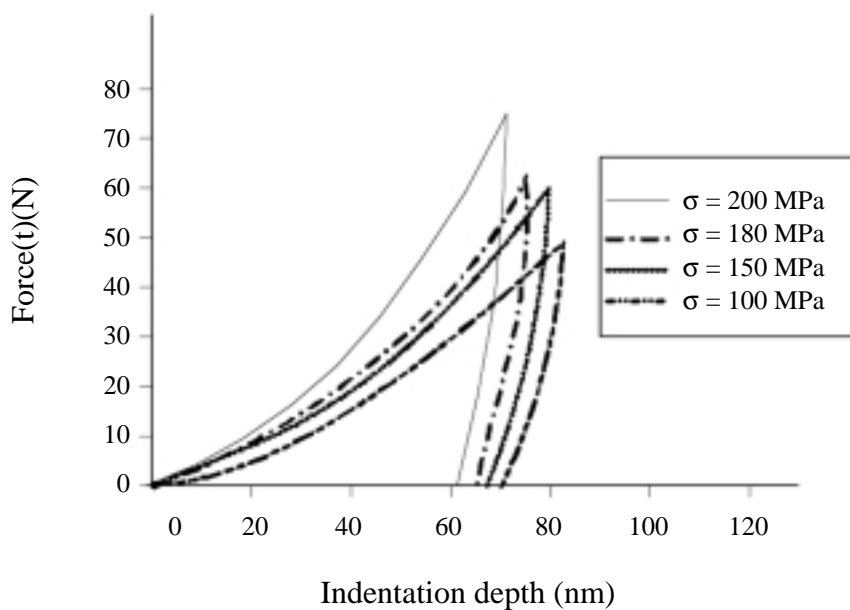


**Figure 4.** The force indentation depth curve for the finite element simulation of various yield strength.

Next, we were to find the best-fit material parameters by matching the experimentally measured transient reaction force with the corresponding of Equation (2). Figure 4 shows an equivalent force indentation depth curve obtained using the equivalent 2D axisymmetric model. In this test, the indentation was done to a depth between 0–100 nm with different force 0–100 N, and various yield strength values. The results showed that peak stress-relaxation nearly matched the peak force at the end of each ramp-displacement, indicating significant interstitial fluid load support, and that stress-relaxation equilibrium occurred when the fluid pressure had subsided. Therefore, the sensitivity of the results to indenter tip sharpness was explored. So, the contact area is not only dependent on the area function of the indenter but also on the elastic-plastic response of the material.

Figures 5 and 6 show the comparison of the effective Poisson's ratio of cartilage in axial compression and tension for one-step ramp loading with  $8.0 \mu\text{m}$  at  $1 \text{ (m/s)}$  followed by Equation (3) and (4) into ANSYS. In a ramp compression-relaxation test, the effective Poisson's ratio ( $-\varepsilon_r / \varepsilon_z$ ) decreased monotonically from 0.6 towards a low value of 0.1, regardless of the contact conditions. However, the effective Poisson's ratio was sensitive to the contact conditions in axial tension: for frictionless contact conditions, the ratio slowly changed from 0.6 towards the Poisson's ratio of the nonfibrillar matrix (0.35); for the adhesive contact conditions, it did not change monotonically. Consequently, these results agree with the sense that the ratio is normally larger for tension than for compression, and that the ratio for tension can be greater than 0.5 (Figure 6). The results show a large influence of the contact conditions on the lateral strain of a specimen in tension. At the same time, the effective Poisson's ratio ( $-\varepsilon_r / \varepsilon_z$ ) deviates from the true Poisson's ratio of the tissue, depending on the length/width ratio of the specimen. The large ratio ( $>0.5$ ) shown in Figure 6 were produced by such deviations, rather than a material anisotropy (which is also the reason for large/small Poisson's ratios). Thus, the result (Figure 6) also shows the influence of fluid pressurization on the radial strain in axial tension (for frictionless contact conditions). Then the effective Poisson's ratio was sensitive to the contact conditions in axial tension: for frictionless conditions, the ratio slowly changed from 0.6 toward the Poisson's ratio of the nonfibrillar matrix; for the adhesive contact conditions, it did not change monotonically.

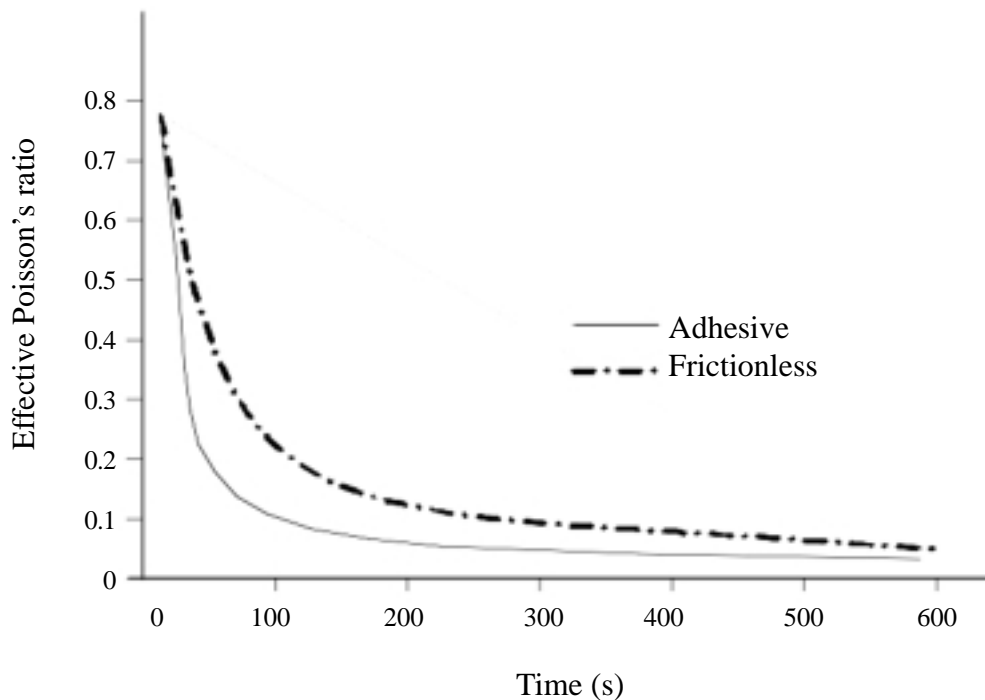


**Figure 5.** Comparison of the effective Poisson's ratio ( $-\varepsilon_r / \varepsilon_z$ ) of cartilage in axial compression for one-step ramp loading.

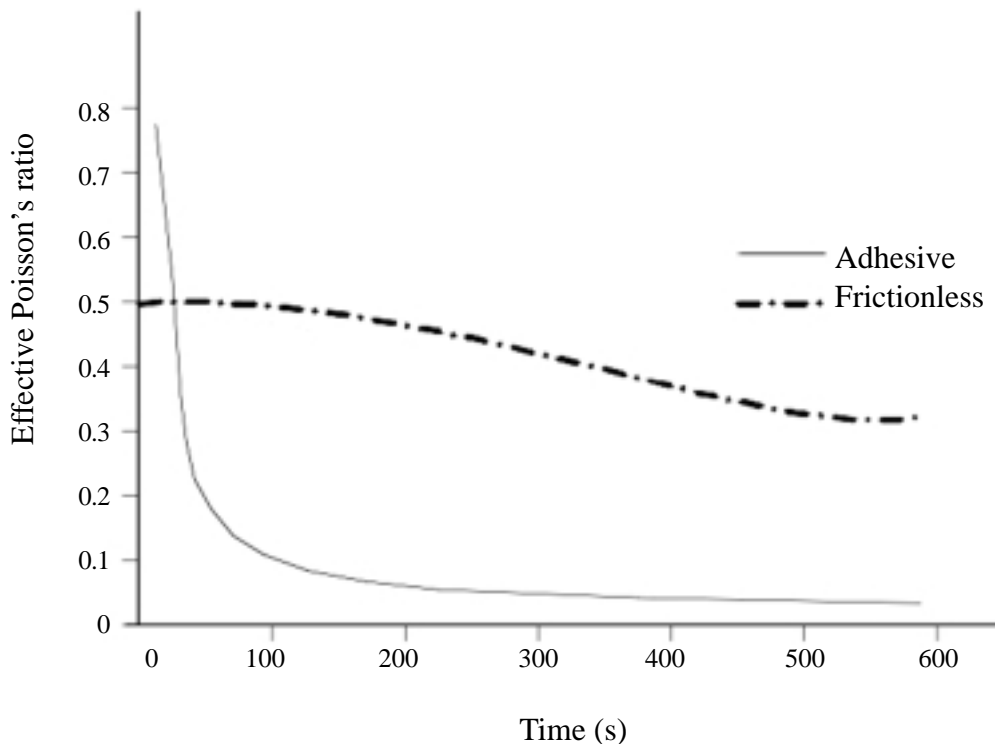


**Figure 6.** Comparison of the effective Poisson's ratio ( $-\varepsilon_r / \varepsilon_z$ ) of cartilage in axial tension for one-step ramp loading.

## CONCLUSION

Collagen fibers are structural elements in articular cartilage. The structure of the collagen network is through to be related to the mechanical stability of the tissue (Minns and Steven, 1977). So, the collagen fibers are oriented to achieve an optimal tangential stiffness of the tissue. The present study was intended to investigate the dependence of the material properties of articular cartilage on the combination of the collagen fiber network structure and the distributed chondrocyte structure. In the nanoindentation test, it suggests that a soft, spheroidal inclusion in a fiber-reinforced structure such as articular cartilage with collagen fibers and chondrocytes gives different material properties depending on the shape of the spheroidal inclusions. Therefore, the investigation illustrates that the variations in the computed ground deformations depend on the degree of stiffness anisotropy (including effects of Poisson's ratio) and the relative magnitudes of horizontal and vertical stress change.

## REFERENCES

- Donzelli, P., R. Spilker, and V. C. Mow. 1999. Contact analysis of biphasic transversely isotropic cartilage layers and correlations with tissue failure. *J. Biomech.* 32: 1037–1047.
- Garcia, J., N. Altiero, and R. Haut. 1998. Approach for the stress analysis of transversely isotropic biphasic cartilage under impact load. *ASME J. of Biomech. Eng.* 120: 608–613.
- Guilak, F., A. Ratcliffe, and V. C. Mow. 1995. Chondrocyte deformation and local tissue strain in articular cartilage: a confocal microscopy study. *J. Ortho. Res.* 13: 410–421.
- Holmes, M., and V.C. Mow. 1990. Nonlinear characteristics of soft gels and hydrated connective tissues in ultrafiltration. *J. Biomech.* 23: 1145–1156.
- Huang, C. Y., V. C. Mow, and G. A. Ateshian. 2001. The role of flow-independent viscoelasticity in the biphasic tensile and compressive responses of articular cartilage. *ASME J. of Biomech. Eng.* 123: 410–417.

- Jones, W., H. T. Beall, G. Lee, S. Kelley, R. Hochmuth, and F. Guilak. 1997. Mechanical properties of human chondrocytes and chondrons from normal and osteoarthritic cartilage. *Trans. of Orthop. Res. Soc.* 22(1): 199.
- Khalsa, P. S., and S. R. Eisenberg. 1997. Compressive behavior of articular cartilage is not completely explained by proteoglycan osmotic pressure. *J. Biomech.* 30: 589–594.
- Kwan, M., W. Lai, and V. C. Mow. 1990. A finite deformation theory for cartilage and other soft hydrated connective tissues. *J. Biomech.* 23: 145–155.
- Lee, K. M., and R. K. Rowe. 1989. Deformations caused by surface loading and tunneling: the role of elastic anisotropy. *Geo-technique* 39(1): 125–140.
- Li, L. P., and W. Herzog. 2004. The role of viscoelasticity of collagen fibers in articular cartilage: theory and numerical formulation. *Biorheology* 41: 181–194.
- Minns, R., and F. Steven. 1977. The collagen fibril organization in human articular cartilage. *J. Anatomy* 123: 437–457.
- Missirilis, Y. F., and A. D. Spiliotis. 2002. Assessment of techniques used in calculating cell-materials interactions. *Biomolec. Eng.* 119: 287–294.
- Mow, V. C., S. C. Kuei, W. M. Lai, and C. G. Armstrong. 1980. Biphasic creep and stress relaxation of articular cartilage: theory and experiment. *ASME J. of Biomech. Eng.* 102: 73–84.
- Pin, G., E. Huang, D. Christiansen, and F. Silver. 1997. Effect of static axial strain on the tensile properties and failure mechanisms of self-assembled collagen fibers. *J. App. Polymer Sci.* 63: 1429–1440.
- Qiu, Y., and G. Weng. 1990. On the application of Mori-Tanaka's theory involving transversely isotropic spheroidal inclusions. *Int. J. Eng. Sci.* 28: 1121–1137.
- Sasaki, N., and S. Odajima. 1996. Stress-strain curve and Young's modulus of a collagen molecule as determined by the X-ray diffraction technique. *J. Biomech.* 29: 655–658.
- Stockwell, R. 1979. *Biology of cartilage cells.* Cambridge University Press, UK.